

Conductivity anisotropy in the antiferromagnetic state of iron pnictides

B. Valenzuela,^{*} E. Bascones,[†] and M.J. Calderón[‡]

Instituto de Ciencia de Materiales de Madrid, ICMM-CSIC, Cantoblanco, E-28049 Madrid (Spain).

(Dated: October 16, 2018)

Recent experiments on iron pnictides have uncovered a large in-plane resistivity anisotropy with a surprising result: the system conducts better in the antiferromagnetic x direction than in the ferromagnetic y direction. We address this problem by calculating the ratio of the Drude weight along the x and y directions, D_x/D_y , for the mean-field $\mathbf{Q} = (\pi, \mathbf{0})$ magnetic phase diagram of a five-band model for the undoped pnictides. We find that D_x/D_y ranges between $0.2 < D_x/D_y < 1.7$ for different interaction parameters. Large values of the orbital ordering favor an anisotropy opposite to the one found experimentally. On the other hand, D_x/D_y is strongly dependent on the topology and morphology of the reconstructed Fermi surface. Our results point against orbital ordering as the origin of the observed conductivity anisotropy, which may be ascribed to the anisotropy of the Fermi velocity.

PACS numbers: 75.10.Jm, 75.10.Lp, 75.30.Ds

Understanding the magnetic state of iron pnictides is probably the starting point to understand the origin of superconductivity in these compounds. The magnetic state is metallic, in contrast to the Mott-insulating behavior of cuprates, and it presents $Q = (\pi, 0)$ columnar ordering: antiferromagnetic in the x direction and ferromagnetic in the y direction. The measured magnetic moment is unexpectedly small and a structural transition occurs at or very close to the magnetic transition [1].

Recent experiments [2–4] have measured an anisotropic resistivity in the magnetic state with unexpected results: The resistivity is smaller in the antiferromagnetic x direction than in the ferromagnetic y direction. A priori the opposite would be expected. The anisotropy extends to finite frequencies as seen in optical conductivity experiments [5, 6]. Surprisingly, the resistivity anisotropy grows with doping and is largest close to the border of the antiferromagnetic phase when the magnetism and the structural distortion are weaker. The anisotropy cannot be explained by the small changes in the lattice constants produced by the structural transition as the lattice constant is larger in the direction with larger conductivity [7]. It can neither be ascribed to the scattering rate of the carriers which has been observed to increase along the x direction and decrease along the y direction in the magnetic state [5], as expected on the basis of scattering by spin fluctuations [8].

The anisotropy of the magnetic state has also been reported in other experiments: (i) Neutron scattering measurements [9] were described with anisotropic exchange constants; (ii) angle resolved photoemission spectroscopy (ARPES) finds a predominant zx orbital component at the Fermi surface at Γ [10]; and (iii) spectroscopic imaging scanning tunneling microscopy experiments [11] were interpreted in terms of one-dimensional bands and of electronic nanostructures aligned along the x -axis.

The origin of the anisotropy is at the center of a hot debate. Orbital ordering (OO) in the d_{zx} and d_{yz} orbitals

has been proposed [5, 8, 11–18] and found in the magnetic state in several theoretical approaches [13, 14, 19, 20]. On the other hand, the $(\pi, 0)$ -antiferromagnetism breaks the tetragonal symmetry and could induce anisotropy without invoking other electronic sources [4, 21, 22]. Within this context it is crucial to uncover the origin of the experimentally observed anisotropies.

In a former work we have calculated the mean field phase diagram of the magnetic state [19] for a five-orbital model [23]. Two different metallic states have been found: the so-called high moment (HM) and low moment (LM) states. In the HM state all the orbital magnetizations point in the same direction leading to a large local magnetic moment, except for the smallest values of U which give a magnetic solution [see Fig. 1(a)]. On the contrary, the LM state consists of antiparallel orbital magnetizations which add up to a small total magnetization. This state, stabilized by the anisotropy of the interorbital exchange interactions, has also been found in other mean-field [24] and LDA+U [25] calculations.

OO defined in terms of a different occupation of d_{yz} and d_{zx} , $n_{yz} - n_{zx}$, is present in both the LM and HM states [see Fig. 1(c)]. The orbital polarization of the Fermi surface shows larger zx orbital component around Γ [19] in agreement with experiments [10]. Whether the zx polarization of the Fermi surface requires strong OO, i.e. finite $n_{yz} - n_{zx}$, or it is just a consequence of the orbital reorganization at the Fermi surface due to the coupling between spin and orbitals is currently under discussion [8, 22]. Furthermore, we estimated the anisotropy of the exchange interactions by mapping the multi-orbital mean field state to a Heisenberg model, and found a large anisotropy only in the LM state showing no correlation with the magnitude of the OO [19].

In this letter we calculate the ratio of the Drude weight D_x/D_y and analyze how it correlates with the presence of OO for the metallic region of a five-orbital $Q = (\pi, 0)$ mean-field phase diagram to unveil the possi-

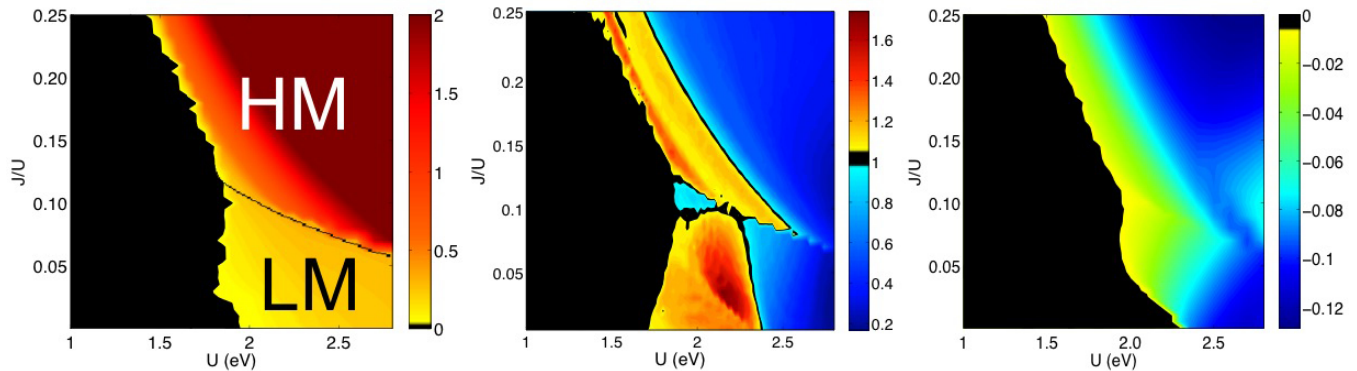


FIG. 1: (Color online) (a) U vs J/U magnetic phase diagram superposed to the magnetization showing the paramagnetic (black), high moment (HM) and low moment (LM) magnetic phases. The magnetic moment reaches values as high as $3.4 \mu_B$. The color scale emphasizes the region with magnetic moments smaller than $2 \mu_B$. (b) Drude ratio with largest values of $D_x/D_y > 1$ corresponding to small values of the magnetization. (c) Orbital ordering $n_{yz} - n_{zx}$. It correlates well with the difference between the partial density of states of d_{yz} and d_{zx} at the Fermi level, see supplementary material.

ble source of the transport anisotropy observed in pnictides [2–6]. We find a wide range of values for this ratio ($0.2 < D_x/D_y < 1.7$) depending on the value of the interaction parameters. Larger OO appears together with larger conductivity in the ferromagnetic direction, therefore it cannot be responsible for the observed anisotropy. We show that the magnitude of the Drude anisotropy is related to the topology and morphology of the Fermi surface. The observed conductivity anisotropy may be ascribed to the Fermi velocity, as in Ref. [4].

The 5-orbital interacting model Hamiltonian and mean-field U vs J/U $\mathbf{Q} = (\pi, \mathbf{0})$ magnetic phase diagram were described in detail in Ref. [19]. As detailed in Ref. [23], both direct Fe-Fe and indirect (via As) hoppings, calculated within the Slater-Koster framework [26], determine the magnitude of the hopping amplitudes which depend on the angle α formed by the Fe-As bonds and the Fe-plane. Here we use $\alpha = 35.3^\circ$ corresponding to a regular As tetrahedra. Energy units are $\sim 1eV$. The interactions include the intraorbital Hubbard U , the Hund’s coupling J , and the interorbital $U' = U - 2J$. The Hamiltonian is solved at the mean-field level keeping only the spin and orbital-diagonal average terms. In Fig. 1(a) we reproduce the phase diagram in the metallic region ($U \leq 2.8$ eV) superposed to the resulting magnetization. As discussed above, HM and LM solutions arise for high and low values of J and both show OO, see Fig. 1(c). OO observed here has the same sign as the one obtained in LDA+U [13] and LDA+DMFT [16].

The Drude weight involves the carrier velocity, the spectral weight, and the scattering rate. Experimentally, the scattering rate is anisotropic, but with an anisotropy opposite to that of the resistivity [5]. Here we neglect the influence of the scattering rate. This approximation allows us to determine the role of the Fermi velocity in

the observed transport anisotropy. We calculate

$$D_x/D_y = \frac{\sum_{\mathbf{k},n} v_x^2(\mathbf{k},n)g(\mathbf{k},n)\delta(\epsilon_n(\mathbf{k}) - E_F)}{\sum_{\mathbf{k},n} v_y^2(\mathbf{k},n)g(\mathbf{k},n)\delta(\epsilon_n(\mathbf{k}) - E_F)} \quad (1)$$

with v_i the velocity in the direction $i = x, y$, n the band index, g the spectral weight, ϵ_n the energy of the band n , δ the Dirac function, E_F the Fermi energy, and the sum in \mathbf{k} restricted to the Fermi surface. The result for the Drude weight ratio is shown in Fig. 1(b). In the paramagnetic (PM) region, black region in the magnetic phase diagram Fig. 1(a), $D_x/D_y = 1$ as expected (discrepancies along the boundary region might be due to numerical precision). The magnetic phases show anisotropy in the Drude weight with ratios $0.2 < D_x/D_y < 1.7$. $D_x/D_y > 1$, consistent with the experimentally observed transport anisotropy [2–4], is observed within a great part of the LM region for intermediate values of the on-site interaction well suited for describing pnictides. In the HM phase, $D_x/D_y > 1$ is restricted to a region close to the PM phase, corresponding to the smallest values of the magnetic moment. Interestingly, in a wide part of the region with $D_x/D_y > 1$ an increase of the anisotropy correlates with a decrease of the magnetic moment. On the other hand $D_x/D_y > 1$ happens to be when the OO is small ($|n_{yz} - n_{zx}| \lesssim 0.05$). Note that although there is not a perfect one to one correspondence between the anisotropy of the Drude weight [Fig. 1(b)] and the OO [Fig. 1(c)], D_x/D_y decreases with increasing OO in most part of the phase diagram. That is, OO seems to favor a transport anisotropy opposite to the one reported experimentally [4]. This finding rules out OO as the origin of the observed resistivity anisotropy.

We now analyze the Drude weight results on the light of the shape of the reconstructed Fermi surface and the velocity vector on it [4]. These are represented in Fig. 2 in the extended (Fe) Brillouin zone for different points

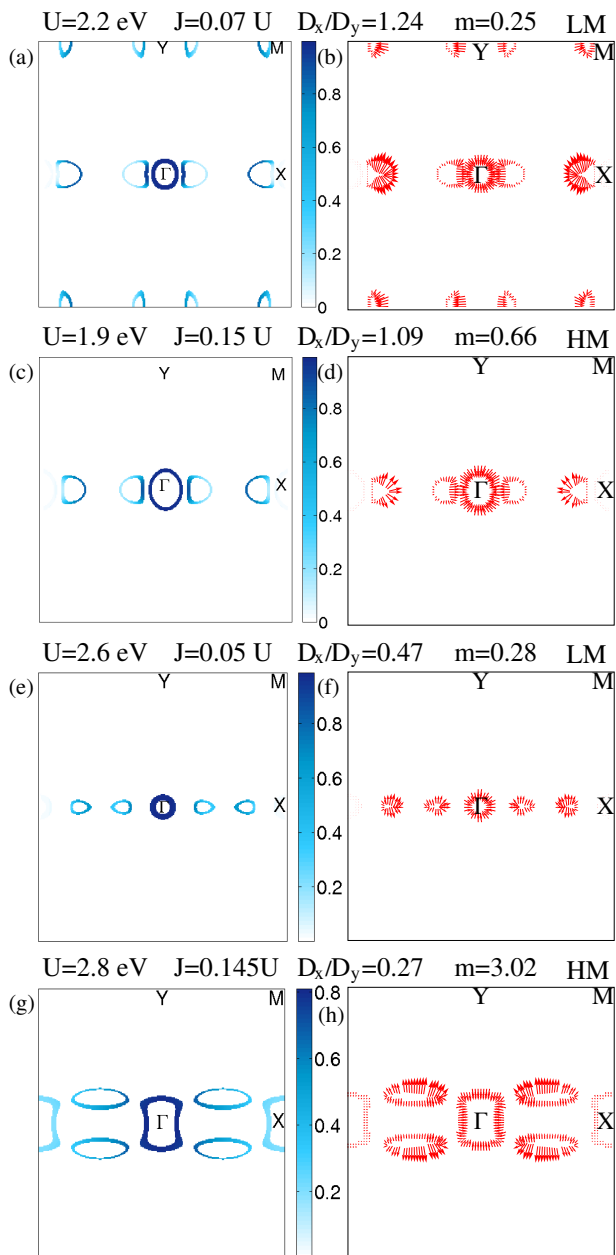


FIG. 2: (Color online) Fermi surfaces (left) and velocities (right) at different points of the phase diagram in the extended (Fe) Brillouin zone. The Fermi surfaces are weighted by their spectral weight. The corresponding U and J values, as well as the obtained anisotropy of the Drude ratio, magnetic moment in Bohr magnetons and the magnetic state appear on top of each figure.

of the phase diagram corresponding to different values of the ratio D_x/D_y . We have chosen Fermi surfaces representative of a wide area of the phase diagram, while other topologies have also been found. We observe a strong dependence of the morphology and topology of the Fermi surfaces on the interaction parameters. These variations, which have a correspondence with the calculated Drude

weight ratio, can be understood starting from the PM Fermi surface in Fig. 3(a) and the plot of the bands in Fig. 3(b). The bands are shown for the PM state (in black) and the LM state (in red) for $U = 2.2$ eV and $J/U = 0.07$.

The PM Fermi surface has hole pockets in Γ and M , and electron pockets in X and Y . In the magnetic states, a gap opens at M and Y near E_F but, for small values of the magnetic moment, there are still pockets in $M \rightarrow Y$ though considerably reduced in size with respect to the PM phase, see Fig. 3. This is illustrated in Fig. 2(a) for $U = 2.2$ eV and $J/U = 0.07$ (corresponding to the LM state) and is also representative of the HM state with a small value of the magnetization (region close to the PM phase). This topology of the Fermi surface corresponds to the largest values of the anisotropy $D_x/D_y > 1.2$. A visual inspection of the velocity vectors at k_F in Fig. 2(b) shows that the v_x component of the velocity dominates in this case, with a large contribution from the pockets at $M \rightarrow Y$. $D_x/D_y > 1$ appears also at points of the phase diagram with the Fermi surface represented in Fig. 2(c) for $U = 1.9$ eV and $J/U = 0.15$. The main difference between Figs. 2(a) and (c) is the disappearance of the pockets at $M \rightarrow Y$ in the latter case while the shape of the pockets at Γ and along $\Gamma \rightarrow X$ is maintained. The electron pockets along $\Gamma \rightarrow X$ are associated to two Dirac cones just below E_F as shown in Fig. 3. The morphology of the Fermi pockets at $\Gamma \rightarrow X$ in Figs. 2(a) and (c) also supports $D_x/D_y > 1$ as evidenced in Fig. 2(d). It is not straightforward to make a connection between the anisotropy of the Drude weight and the orbital content of the Fermi pockets. The pockets close to Y show zx and xy polarization [23], while in the Dirac cone electron pocket the v_x contribution comes mostly from the d_{yz} polarized segment closer to Γ [19]. In fact, the anisotropy of the Drude conductivity cannot be ascribed to the orbital reorganization at E_F , whose dependence on U and J follows that of the OO, see supplementary material.

Now we turn to Fig. 2(e) (for $U = 2.6$ eV and $J/U = 0.05$). The topology of the Fermi surface is maintained with respect to Fig. 2(c) but the morphology is different: the pockets are more isotropic and those close to X have a slightly stronger v_y component rendering $D_x/D_y \lesssim 1$ [see Fig. 2(f)]. Finally, Fig. 2(g) (for $U = 2.8$ eV and $J/U = 0.145$) corresponds to a strong anisotropy $D_x/D_y \ll 1$, opposite to the one observed experimentally. The pockets along $\Gamma \rightarrow X$ have disappeared. Two ellipsoidal pockets with a strong v_y component close to this direction are observed instead, see Fig. 2(f).

The Fermi surfaces in Fig. 2(a) and (c), once folded to the FeAs Brillouin zone and taken into account the existence of magnetic domains, resemble the flower-like Fermi surfaces observed in ARPES in the magnetic state [27, 28]. From the available experimental results we cannot conclude on the presence or absence of Fermi pockets close to Y .

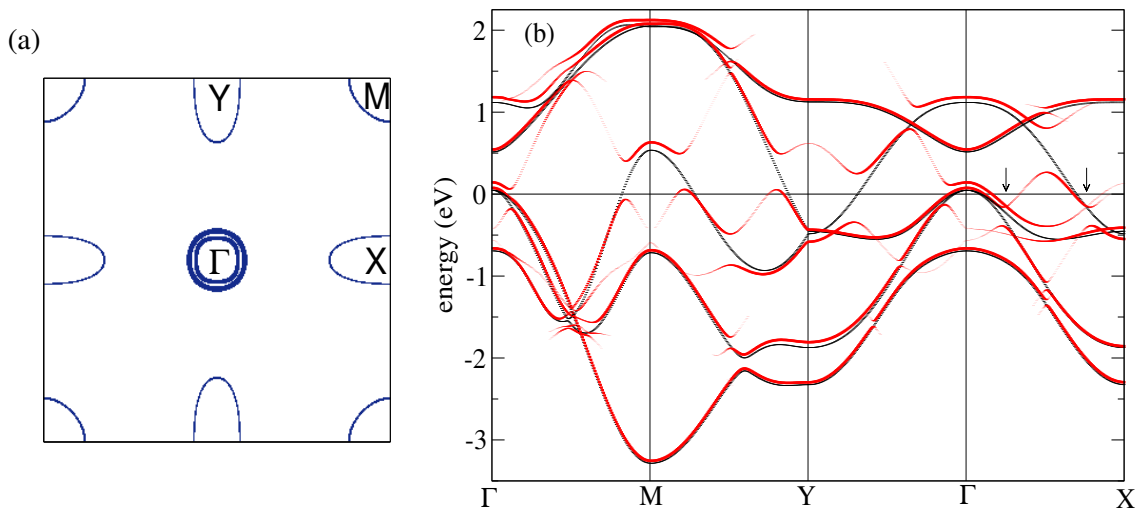


FIG. 3: (Color online) (a) Fermi surface in the paramagnetic state for $U, J = 0$. (b) Band structure for $U = 2$ eV and $J/U = 0.07$ corresponding to the LM state, in red. The linewidth gives a measure of the spectral weight. The paramagnetic bands, in black, are shown as a reference. The position of the Dirac cones along ΓX is marked with arrows.

In conclusion, we have found that the anisotropy of the Fermi velocity which is strongly related to the morphology and topology of the reconstructed Fermi surface results in large variations in the ratio of the Drude weight. Depending on the shape of the Fermi surface the resistivity can be larger in the antiferromagnetic x or the ferromagnetic y direction. Larger orbital ordering correlates with a resistivity anisotropy opposite to the one observed, i.e. larger conductivity in the ferromagnetic y direction. A larger conductivity in the antiferromagnetic x direction, consistent with the experimentally observed conductance anisotropy, corresponds to Fermi surfaces whose shape resembles those observed experimentally. Values of the anisotropy $D_x/D_y > 1.2$ are achieved when the Fermi surface has pockets at Y in the extended Fe Brillouin zone. Pockets around Y are also predicted in ab-initio [21] and mean field calculations [29, 30]. The electron pockets originating from the Dirac cones can also govern the anisotropy when $D_x/D_y > 1$. The region of the phase diagram with $D_x/D_y > 1$ shows a small magnetic moment, as observed experimentally.

We acknowledge funding from Ministerio de Ciencia e Innovación through Grants No. FIS 2008-00124/FIS, and No. FIS2009-08744 and Ramón y Cajal contract, and from CSIC through Grants PIE-200960I033 and PIE-200960I180.

* Electronic address: belenv@icmm.csic.es

† Electronic address: leni@icmm.csic.es

‡ Electronic address: calderon@icmm.csic.es

[1] J. Zhao, et al., Nature Materials **7**, 953 (2008).

[2] J.-H. Chu, et al., Phys. Rev. B **81**, 214502 (2010).

[3] J.-H. Chu, et al., Science **329**, 824 (2010).

[4] M. Tanatar, et al., Phys. Rev. B **81**, 184508 (2010).

[5] A. Dusza, et al., arXiv:1007.2543 (2010).

[6] M. Nakajima, Poster at SNS2010 conference (2010).

[7] Q. Huang, et al., Phys. Rev. B **78**, 054529 (2008).

[8] C.-C. Chen, et al., arXiv:1004.4611 (2010).

[9] J. Zhao, et al., Nature Physics **5**, 555 (2009).

[10] T. Shimojima, et al., Phys. Rev. Lett. **104**, 057002 (2010).

[11] T.-M. Chuang, et al., Science **327**, 181 (2010).

[12] R. R. P. Singh, arXiv:0903.4408 (2009).

[13] C.-C. Lee, W.-G. Yin, and W. Ku, Phys. Rev. Lett. **103**, 267001 (2009).

[14] F. Krüger, et al., Phys. Rev. B **79**, 054504 (2009).

[15] J. Wu, P. Phillips, and A. H. Castro Neto, Phys. Rev. Lett. **101**, 126401 (2008).

[16] Z. P. Yin, K. Haule, and G. Kotliar, arXiv:1007.2867 (2010).

[17] W. Lv, F. Krüger, and P. Phillips, Phys. Rev. B **82**, 045125 (2010).

[18] W.-G. Yin, C.-C. Lee, and W. Ku, Phys. Rev. Lett. **105**, 107004 (2010).

[19] E. Bascones, M. J. Calderón, and B. Valenzuela, Phys. Rev. Lett. **104**, 227201 (2010).

[20] M. Daghofer, et al., Phys. Rev. B **81**, 014511 (2010).

[21] S.A.J. Kimber, D.N. Argyriou, I.I. Mazin arXiv:1005.1761 (2010).

[22] M. Daghofer, et al., Phys. Rev. B **81**, 180514 (2010).

[23] M. J. Calderón, B. Valenzuela, and E. Bascones, Phys. Rev. B **80**, 094531 (2009).

[24] M. Luo, et al., arXiv:1007.1436 (2010).

[25] F. Cricchio, O. Granas, and L. Nordstrom, Phys. Rev. B **80**, 140403 (2010).

[26] J. Slater and G. Koster, Phys. Rev. **94**, 1498 (1954).

[27] T. Kondo, et al., Phys. Rev. B **81**, 060507(R) (2010).

[28] C. He, et al., arXiv:1001.2981 (2010).

[29] R. Yu, et al., Phys. Rev. B **79**, 104510 (2009).

[30] E. Kaneshita, T. Morinari, and T. Tohyama, Phys. Rev. Lett. **103**, 247202 (2009).